Supporting Information

Ultrafast mechanosynthesis of hydrogen-bonded organic frameworks with UV and NIR photoswitching of photochromic/photothermal behavior

Yanfeng Gao, [a] Zhe Wang, [a] Tieqiang Wang, [a] Junbiao Wu, * [a] Zhuopeng Wang, [a] Zhiqiang Liang, [b] Jiyang Li [b]

[a] Department of Chemistry, College of Sciences, Northeastern University, Shenyang, 110819, P. R. China. E-mail: wujunbiao@mail.neu.edu.cn;

[b] State Key Laboratory of Inorganic Synthesis and Preparative Chemistry, College of Chemistry, Jilin University, Changchun 130012, P. R. China.

Experimental section

Materials and reagents.

All chemicals were purchased from commercial sources without further purification. Oxalic acid dihydrate ($H_2C_2O_4·2H_2O$, AR) and 4,4-bipyridine ($C_{10}H_8N_2$, AR) were purchased from Beijing Innochem Science and Technology Co. Ltd. and ethanol (CH_3CH_2OH, AR) were provided by Tianjin Yongda Chemical Reagent Co. The water used in the experiments was deionized and distilled.

Characterization.

Powder X-ray diffraction (PXRD) patterns were collected in the range 2θ = 4-40° at room temperature using Cu-Kα (λ = 1.5418 Å) radiation with a PANalytical B.V. Empyrean X-ray diffractometer. Visible light response tests were carried out using a xenon lamp model PLS-SXE300/300UV with 420 nm cut-off filter manufactured by Beijing Porphyry Technology Co. UV-Vis diffuse reflectance absorption spectra in the 200-2000 nm range were recorded at room temperature using a Lambda 750s instrument. The UV lamps used in the experiment were UVA (365 nm, 24 W), UVB (311 nm, 20 W) and UVC (254 nm, 16 W). Fourier transform infrared (FT-IR) spectra in the range of 400-4000 cm^{-1}were recorded on a ThermoFisher Nicolet 6700 FT-IR spectrophotometer using KBr pellets. Electron paramagnetic resonance (EPR) was performed on a Bruker magnetech ESR5000 spectrometer. The IR camera was an ut260b (Unit) with an operating temperature range of -15 °C to 550 °C. Thermogravimetric (TG) analysis was carried out on a TA Q500 analyzer in air with a heating rate of 10 °C min^{-1} from room temperature to 800 °C. SEM images were tested using a SU8000 Field Emission Electron Scanning Microscope manufactured by Hitachi High-Technologies, Japan.

Synthesis of MCS-HOF.

MCS-HOF was prepared using a mixture of $H_2C_2O_4·2H_2O$ and $C_{10}H_8N_2$ (molar ratio 2:1), which was ball-milled at 10 to 50 Hz in a planetary ball mill of type KE-0.4 L. During the reaction, 0.02 mmol of $H_2C_2O_4·2H_2O$ and 0.01 mmol of $C_{10}H_8N_2$ were weighed and ball milled in an agate milling jar for different times (10, 20, 30, 40, 50 and 60 s), resulting in a series of samples named MCS-HOF-Frequency-Time and MCS-HOF-Time-Frequency. For the scale-up experiment, the molar ratio of the two substances was maintained at 2:1, a total of 600 g was weighed and ball-milled in a KE-4 L planetary ball mill for 10 seconds at a frequency of 50 Hz resulting in a sample named MCS-HOF-50Hz-10s-Scale up. In all experiments, the ball-to-powder mass ratio was always maintained at 10:1. After grinding, the product was scraped off the wall of the agate grinding jar, sonicated to completely dissolve the impurities, washed three times each with water and ethanol, and the supernatant was removed by centrifugation, and the solid product was finally dried in an oven at 60 °C for 12 h.

The yield was calculated from the number of moles of $C_{10}H_8N_2$ using the following equation.

$$Yield = \frac{m_{sample}}{0.05mmol * M_{HOF}} \times 100\%\#(1)$$

m_{sample} is the mass of MCS-HOF obtained in each experiment, and M_{HOF} is the relative molecular mass of MCS-HOF, which is 336.26 g/mol.

Note S1. The average yield of the synthesis appeared to fluctuate up and down at different milling times. The potential explanations for this phenomenon are as follows:

1. It is inevitable that a certain quantity of the sample will adhere to both the ball mill jar and the ball mill beads. Inevitably, this will result in a certain degree of loss when the process is not processed cleanly, which will consequently introduce a certain degree of inaccuracy in the yield calculation.

2. It is inevitable that a certain amount of sample will adhere to the walls of the beaker and centrifuge tubes during the ultrasonic cleaning and centrifugation processes. This will inevitably lead to a certain amount of error in the calculation of the yield.

3. When processing the supernatant after centrifugation, some of the samples especially the nanosized samples will be brought out with the solution.

The combination of these factors results in the observed fluctuations in yield after different grinding times.

Solvent and thermal stability of MCS-HOF

Solvent and thermal stability are critical to the practical applications of photochromic materials, combining the grinding time and mechanical frequency considerations, MCS-HOF-50Hz-10s was selected for stability testing. After soaking in deionized water and ethanol solution for 7 days, PXRD test was performed, and the results were in good agreement with simulated PXRD (Fig. S7). The thermal stability of MCS-HOF is confirmed by the TG curve (Fig. S8), the structure of MCS-HOF remains intact up to 200 ℃, while it decomposes at 275 ℃, in accordance with the decomposition of oxalate and bpy. The stability of MCS-HOF is able to meet the common practical application scenarios.

Calculation of photothermal conversion efficiency of MCS-HOF-50Hz-10s.

Follwing the methods described in the literature,[1,2] the photothermal conversion efficiency was calculated. The specific calculation steps are as follows:
Considering the total energy balance of the system.

$$\sum_i m_i C_{p,i} \frac{dT}{dt} = Q_s - Q_{loss} \#\ (2)$$

where m_i (0.93 g) and $C_{p,i}$ (0.8 J (g °C)$^{-1}$) are the mass and heat capacity of the system components (MCS-HOF-50Hz-10s sample and quartz glass), respectively. Q_s is the photothermal thermal energy input from the NIR laser irradiation of the MCS-HOF-50Hz-10s sample, while Q_{loss} is the fraction of thermal energy lost to the environment. The system is in equilibrium when the system temperature reaches its maximum value.

$$Q_s = Q_{Loss} = hS\Delta T_{max} \#\ (3)$$

where h is the heat transfer coefficient, S is the surface area of the vessel, and ΔT_{max} is the maximum temperature change. The photothermal conversion efficiency η can be derived from the following equation.

$$\eta = \frac{hS\Delta T_{max}}{I\left(1 - 10^{-A_{808}}\right)} \#（4）$$

where I is the laser power (1.07 W cm^{-2} to ensure that the temperature does not bleach the sample) and A_{808} is the absorbance of the sample at 808 nm (0.41073) (Fig. S15). To obtain hS, an acausal driving force temperature θ was introduced as follows.

$$\theta = \frac{T - T_{surr}}{T_{max} - T_{surr}} \#（5）$$

where T is the temperature of MCS-HOF-50Hz-10s, T_{max} is the maximum system temperature (47.5 °C), and T_{surr} is the initial temperature (23.5 °C). The sample system time constant τ_s can be obtained from the following equation.

$$\tau_s = \frac{\sum_i m_i C_{p,i}}{hS} \#（6）$$

hence

$$\frac{d\theta}{dt} = \frac{1}{\tau_s hS\Delta T_{max}} Q_s - \frac{\theta}{\tau_s} \#(7)$$

When the laser is off, Qs = 0; therefore, $\frac{d\theta}{dt} = -\frac{\theta}{\tau_s}$ and $t = -\tau_s ln\theta$.

Thus hs can be calculated from the slope of the cooling time vs. lnθ (Fig. S17 and Fig. S18). Finally, τ_s is 44.1 s and the photothermal conversion efficiency η is 61.86%.

Supporting Figures

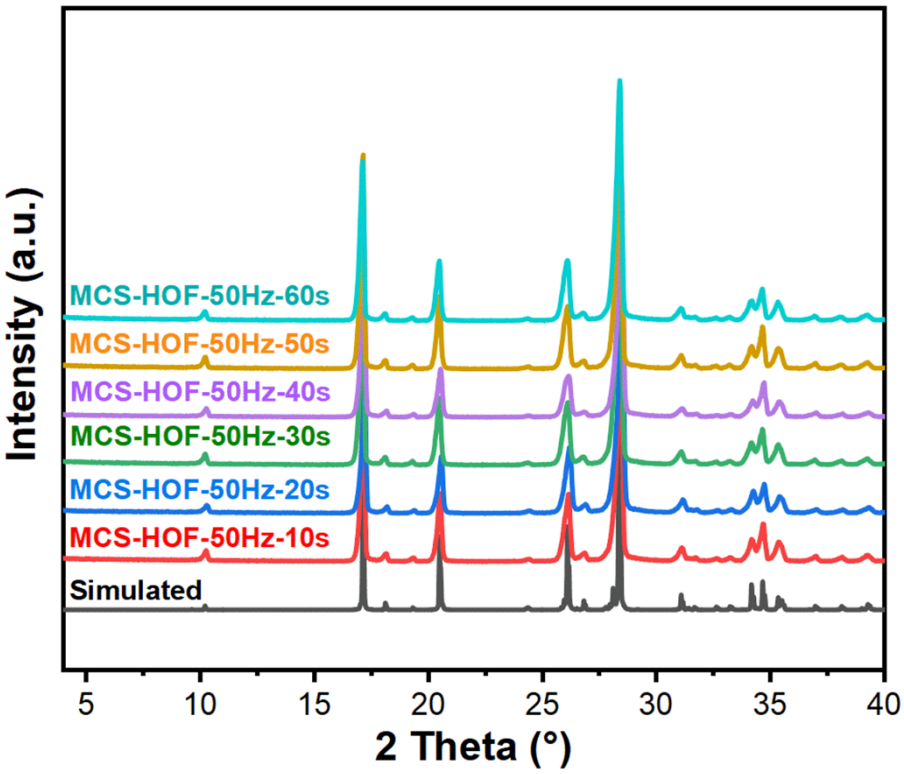

Fig. S1. PXRD of MCS-HOF obtained at a milling frequency of 50 Hz for different reaction times.

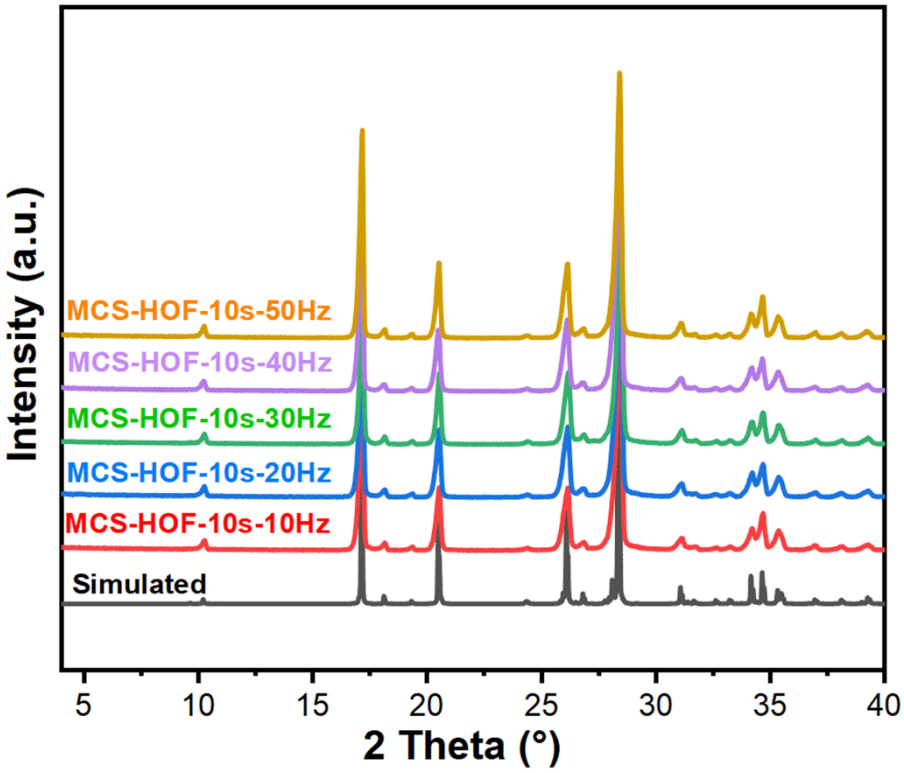

Fig. S2. PXRD of MCS-HOF obtained at different mechanical frequencies with a milling time of 10 s.

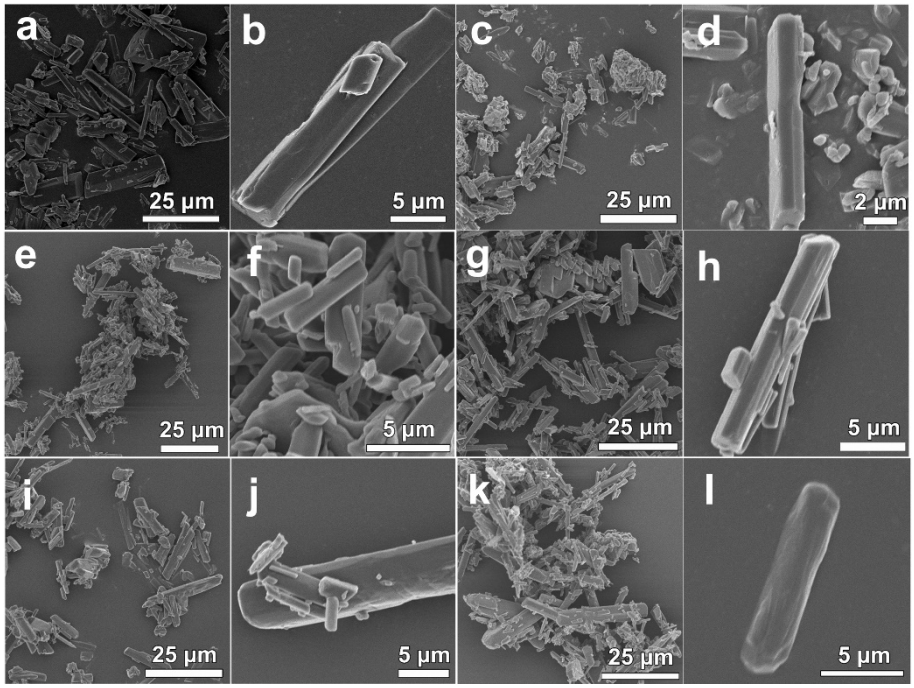

Fig. S3. SEM image of MCS-HOF prepared at a frequency of 50 Hz with different times of milling. (a, b) MCS-HOF-50Hz-10s. (c, d) MCS-HOF-50Hz-20s. (e, f) MCS-HOF-50Hz-30s. (g, h) MCS-HOF-50Hz-40s. (i, j) MCS-HOF-50Hz-50s. (k, l) MCS-HOF-50Hz-60s.

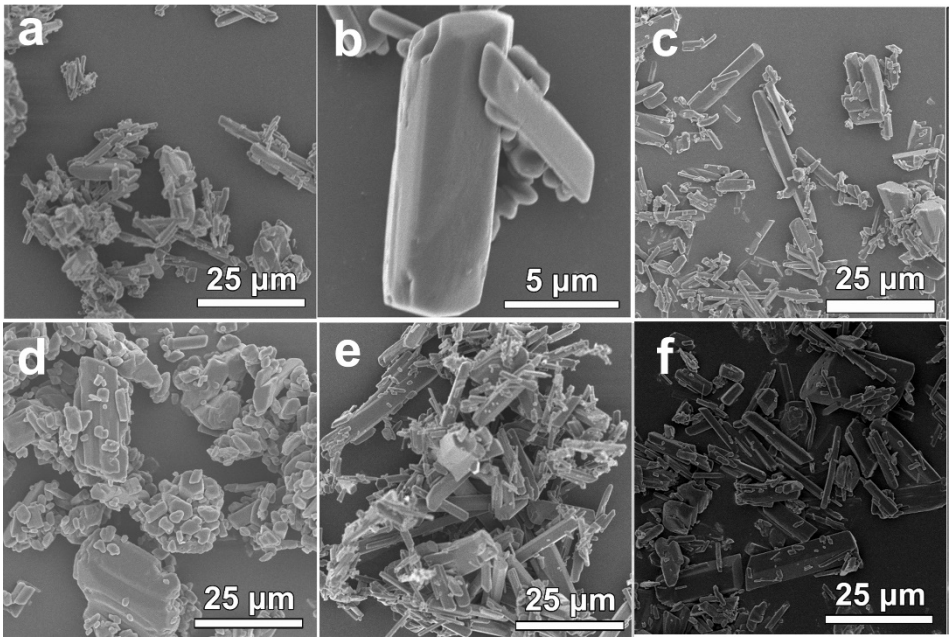

Fig. S4. SEM image of MCS-HOF prepared with a milling time of 10s at different milling frequencies. (a, b) MCS-HOF-10s-10Hz. (c) MCS-HOF-10s-20Hz. (d) MCS-HOF-10s-30Hz. (e) MCS-HOF-10s-40Hz. (f) MCS-HOF-10s-50Hz.

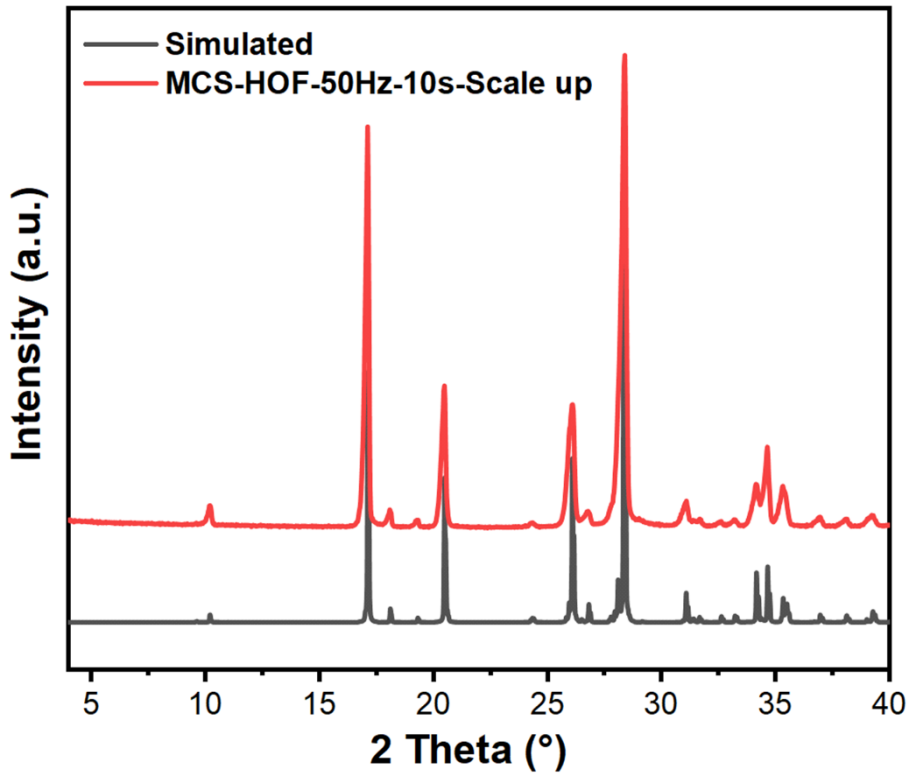

Fig. S5. PXRD spectra of MCS-HOF-50Hz-10s at scale-up.

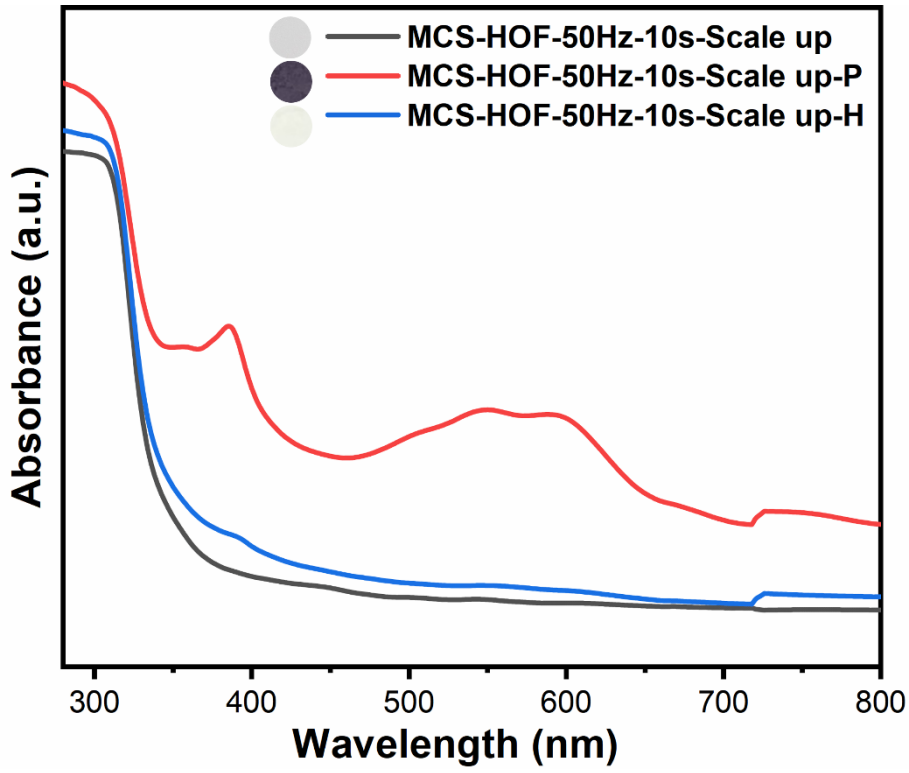

Fig. S6. UV-Vis spectra of the original MCS-HOF-50Hz-10s-Scale up, colored MCS-HOF-50Hz-10s-Scale up-P and faded MCS-HOF-50Hz-10s-Scale up-H.

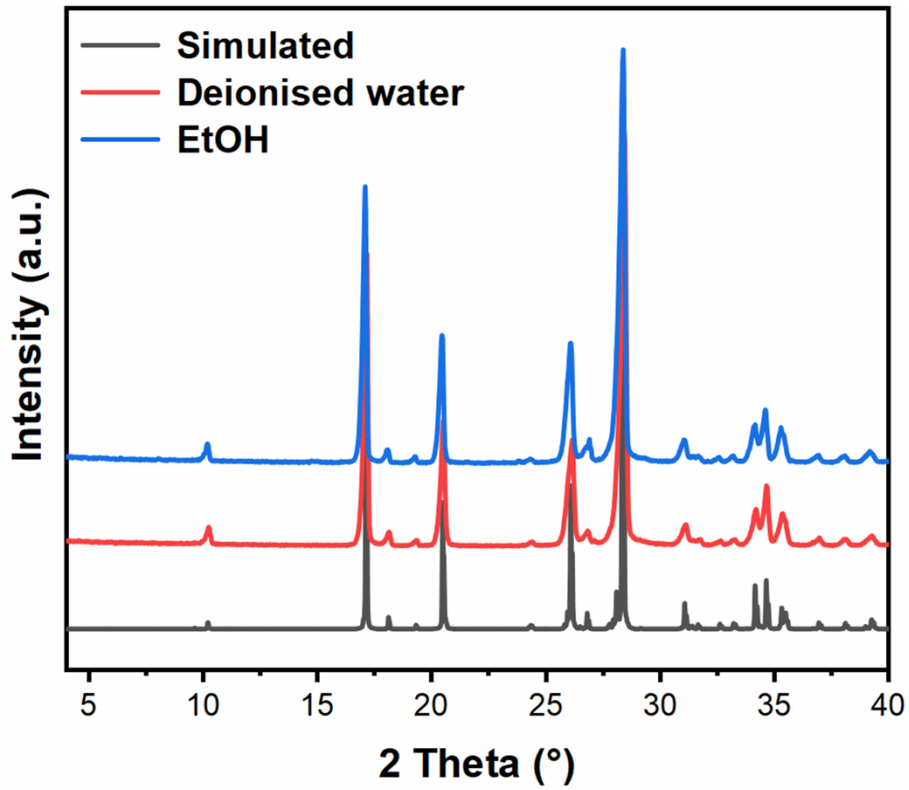

Fig. S7. PXRD of MCS-HOF-50Hz-10s after 7 days immersion in deionized water and EtOH, respectively.

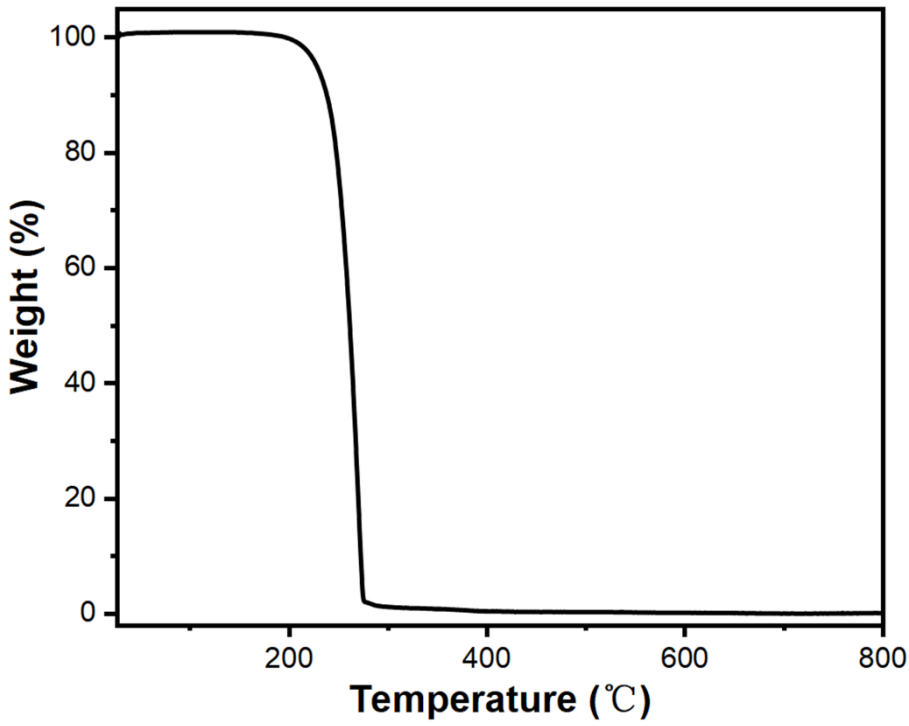

Fig. S8. Thermogravimetric analysis of the MCS-HOF-50Hz-10s in air, warmed up from room temperature to 800 °C at 10 °C/min.

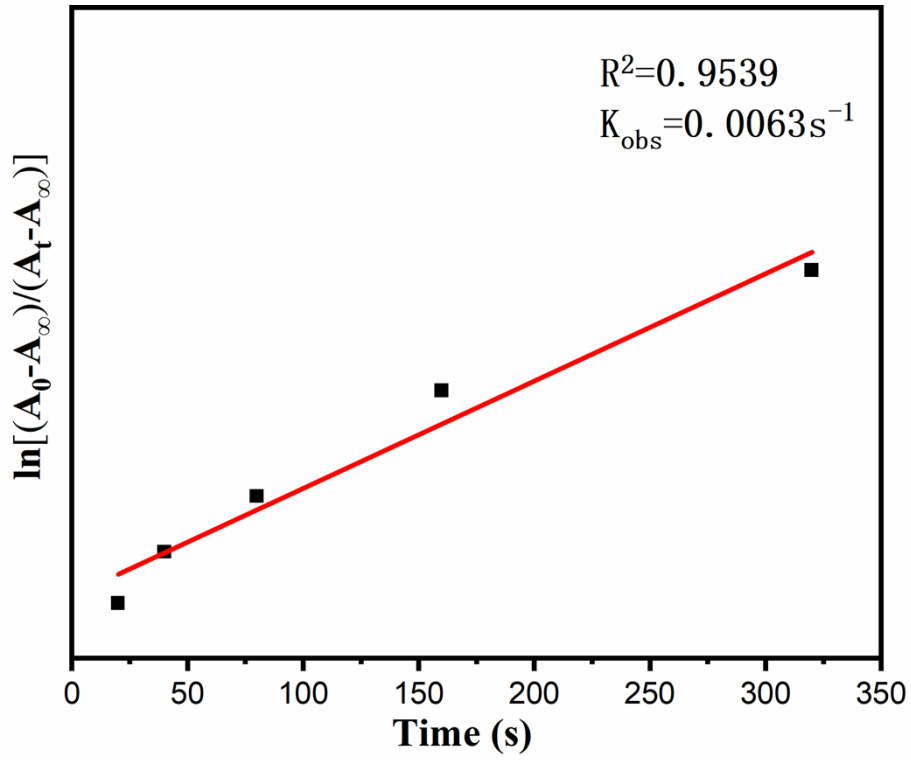

Fig. S9. First-order kinetic plot for change in absorbance at λ = 552 nm, where A_0, A_t, and A_∞ are the absorbance values at time zero, time t, and infinite time of the reaction, respectively.

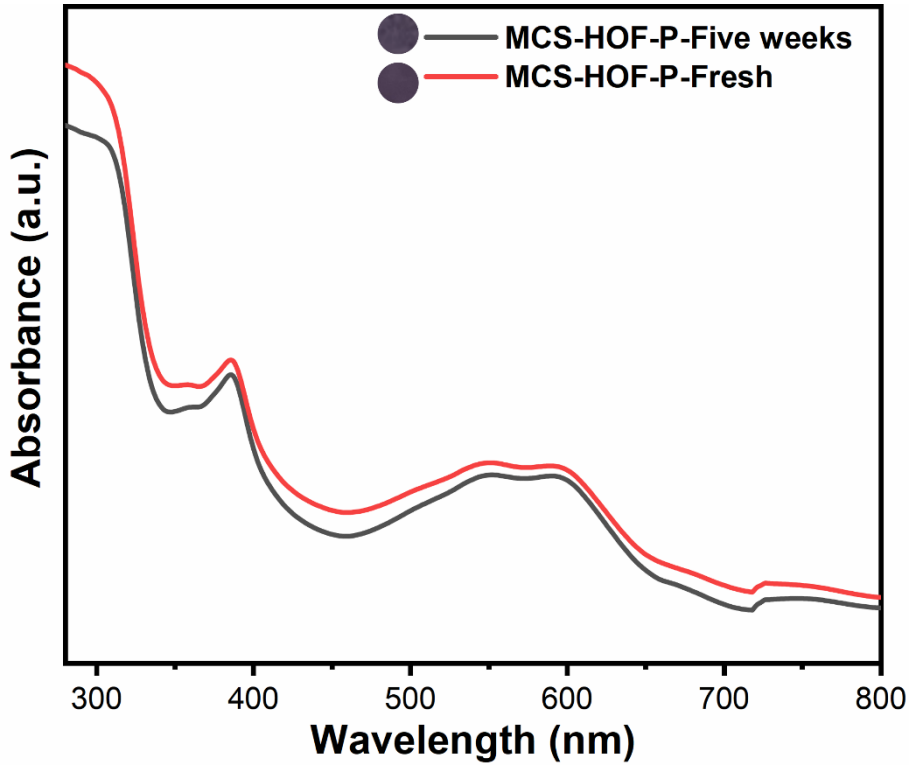

Fig. S10. UV-vis spectra of fresh colored sample (MCS-HOF-P-Fresh) and colored sample after five weeks of environmental storage (MCS-HOF-P-Five weeks) (both irradiation under a 254 nm-16 W UV lamp for 5 min).

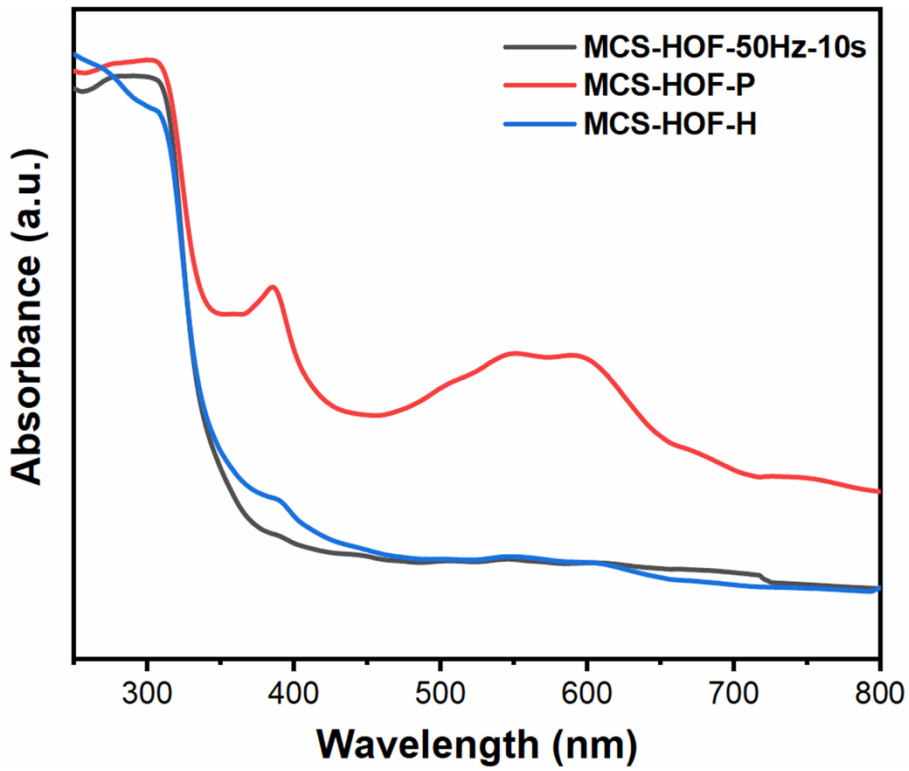

Fig. S11. UV-Vis spectra of the original MCS-HOF-50Hz-10s, photochromic state irradiated at 254 nm-16 W UV lamp (MCS-HOF-P) and faded state (MCS-HOF-H).

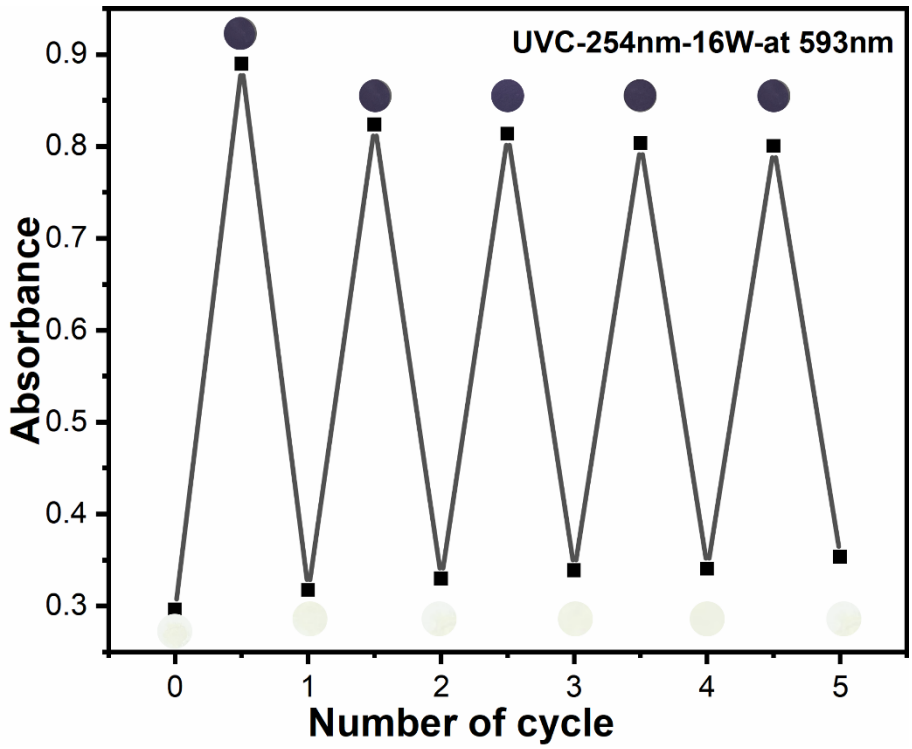

Fig. S12. Reversibility of MCS-HOF (colored state under UVC irradiation and faded state by heating at 100 °C for 30 min) through UV-Vis spectra (monitored at 593 nm of UV-Vis spectra).

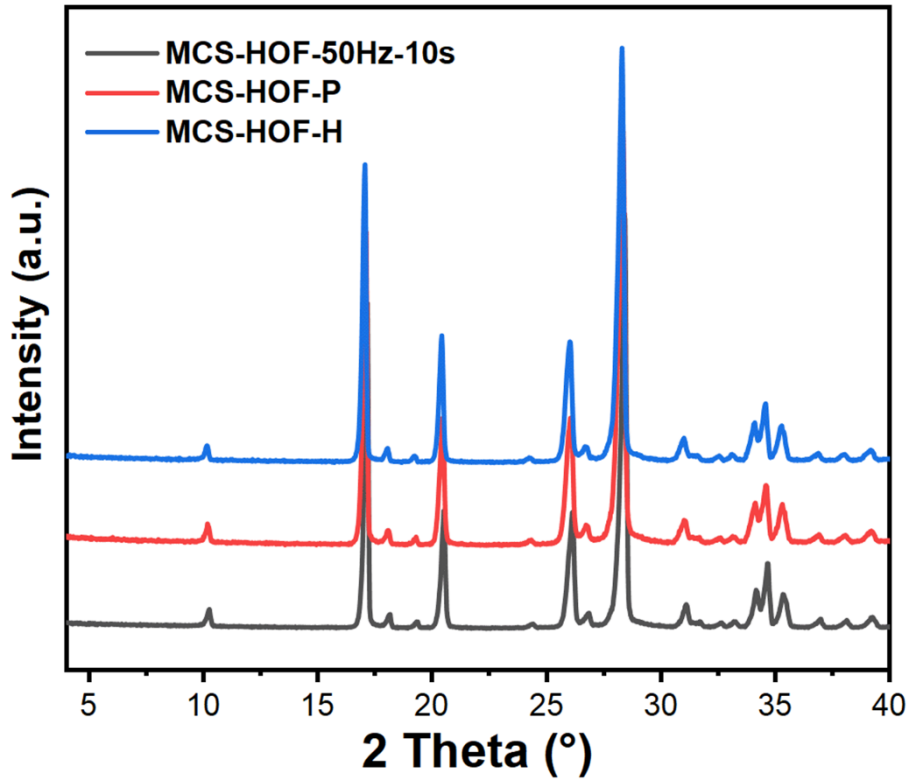

Fig. S13. PXRD of the original MCS-HOF-50Hz-10s, photochromic state irradiated at 254 nm-16 W UV lamp (MCS-HOF-P) and faded state (MCS-HOF-H).

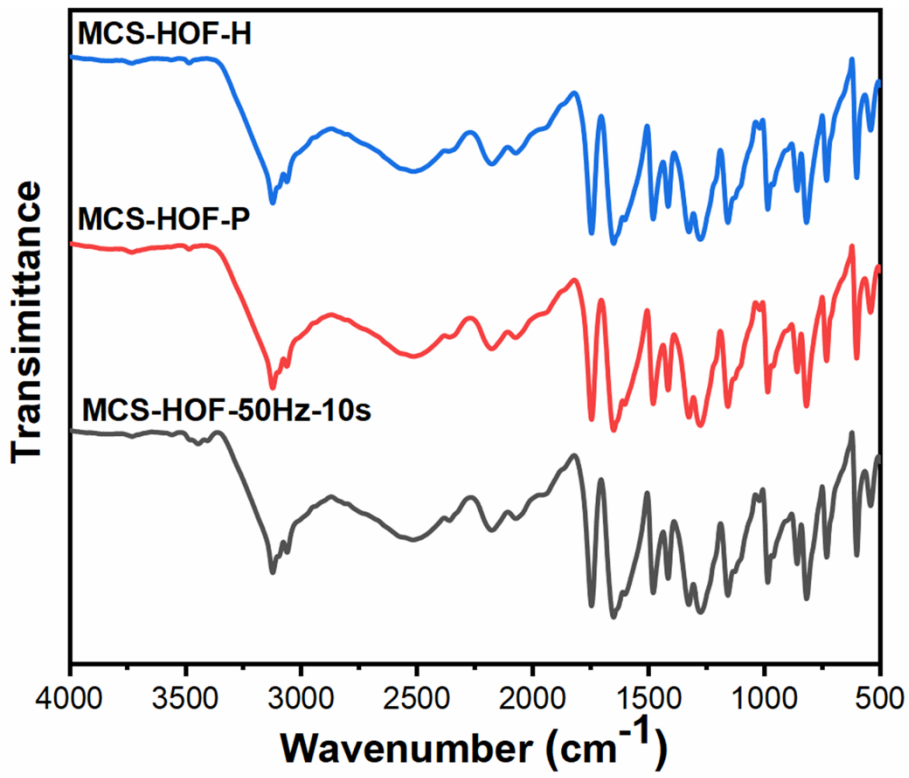

Fig. S14. FTIR spectra of the original MCS-HOF-50Hz-10s, photochromic state irradiated at 254 nm-16 W UV lamp (MCS-HOF-P) and faded state (MCS-HOF-H).

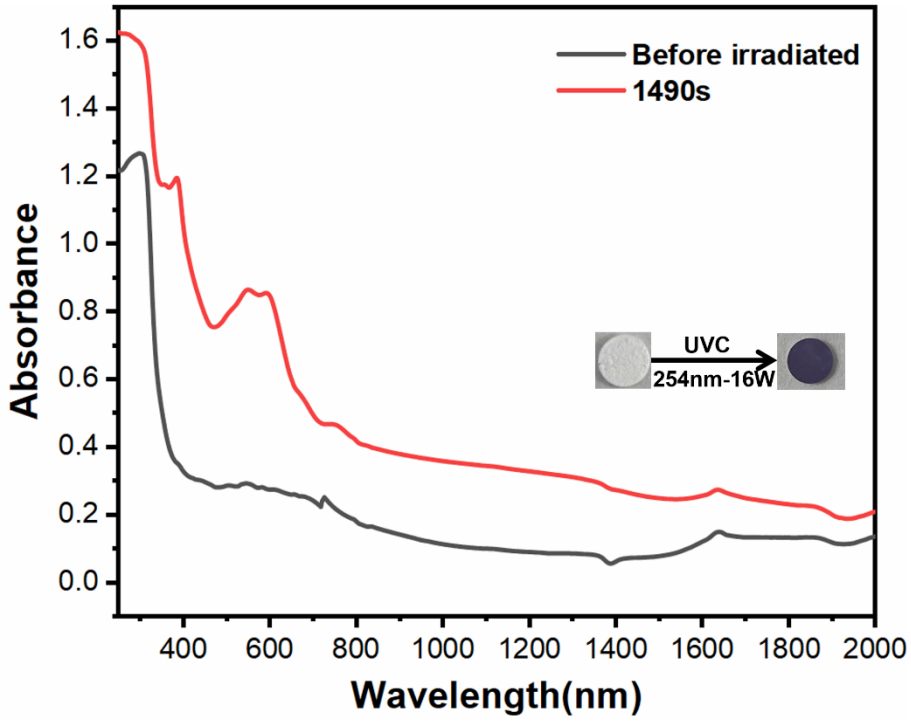

Fig. S15. UV-Vis-NIR spectra and photographs of MCS-HOF-50Hz-10s before and after irradiated under 254 nm-16 W UV lamp.

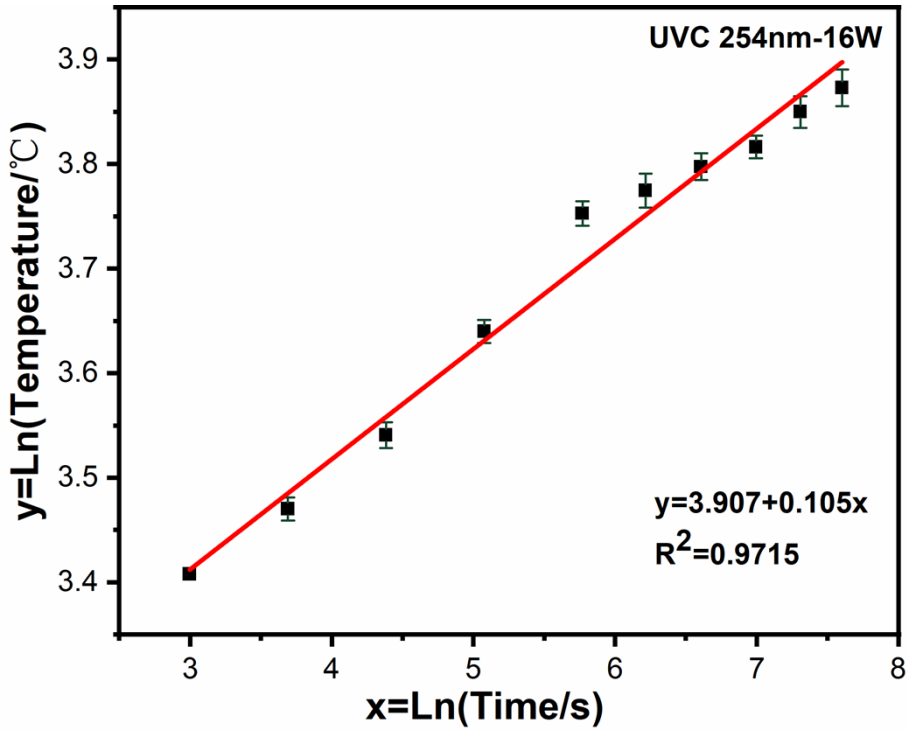

Fig. S16. Linear relationship between photothermal temperature (logarithmic value) and UVC irradiation time (logarithmic value) for MCS-HOF-50Hz-10s.

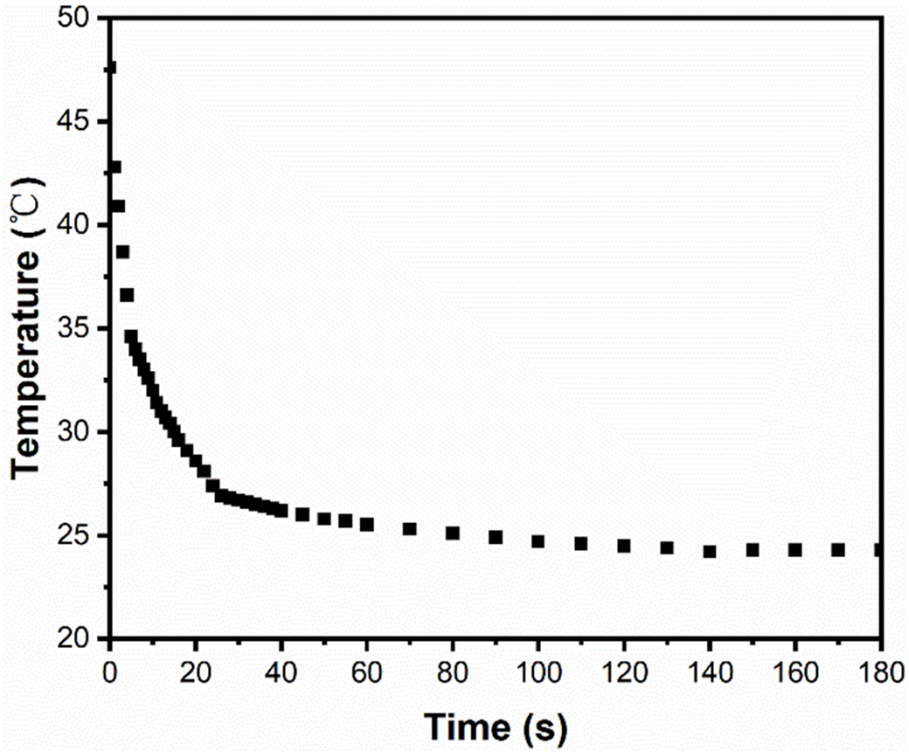

Fig. S17. (a) Cooling curve of MCS-HOF-50Hz-10s after being irradiated under 808 nm light-(1.07 W cm^{-2}).

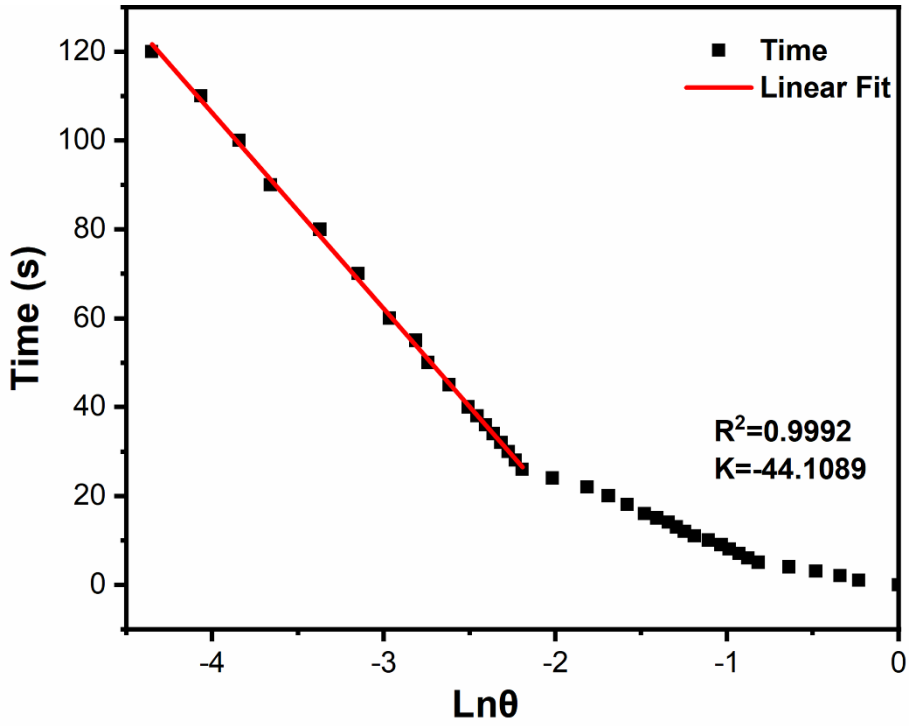

Fig. S18. Fitted plot of linear correlation between cooling time and lnθ.

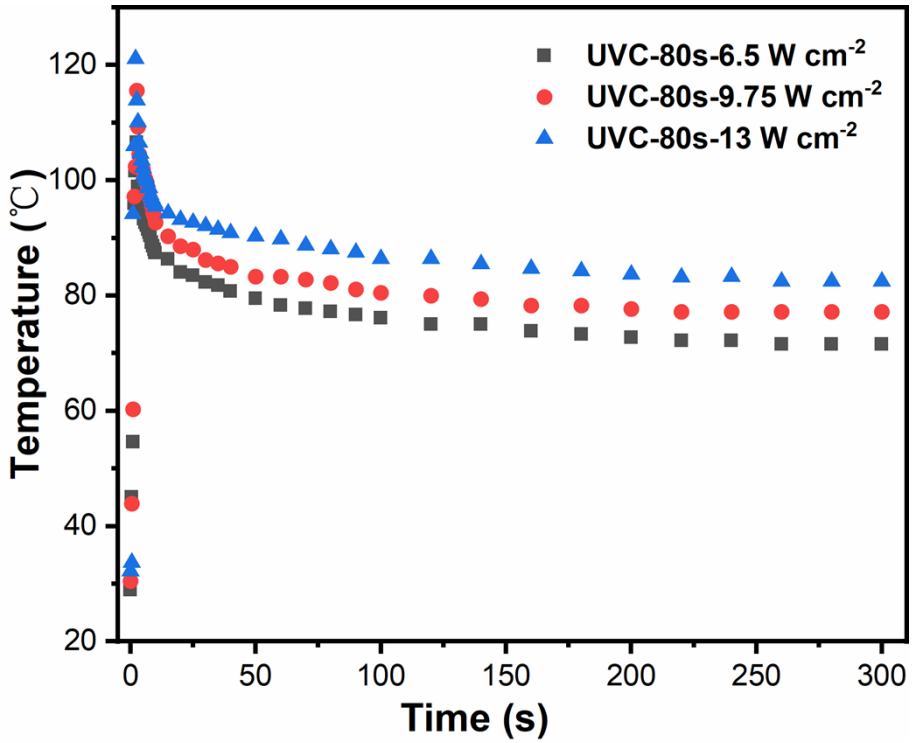

Fig. S19. Temperature changes of MCS-HOF-50Hz-10s after UVC irradiation for 80 s under 808 nm NIR light with different power densities.

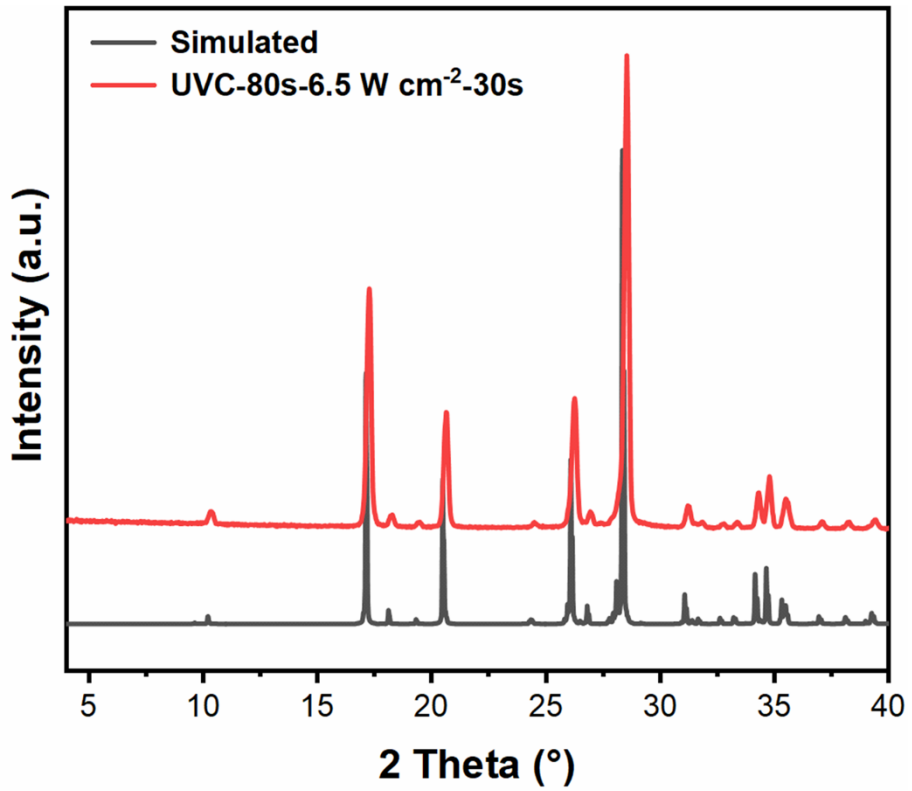

Fig. S20. PXRD of MCS-HOF-50Hz-10s after UVC irradiation for 80 s and then irradiated with 808 nm NIR light at 6.5 W cm^{-2} power density for 30 s.

Supporting Tables

Table S1. MCS-HOF yields at 50 Hz for different reaction times.

Sample	Yield(%)
MCS-HOF-50Hz-10s	94.68
MCS-HOF-50Hz-20s	93.14
MCS-HOF-50Hz-30s	93.98
MCS-HOF-50Hz-40s	92.09
MCS-HOF-50Hz-50s	96.10
MCS-HOF-50Hz-60s	93.40

Table S2. MCS-HOF yields at different mechanical frequencies at 10 s.

Sample	Yield (%)
MCS-HOF-10s-10Hz	84.79
MCS-HOF-10s-20Hz	88.41
MCS-HOF-10s-30Hz	89.72
MCS-HOF-10s-40Hz	91.66
MCS-HOF-10s-50Hz	94.82

Table S3. The synthesis times and yields of the products in this work were compared to previous results in the literature.

NO.	HOFs/MOFs type	Raw Material	Method	Yield(%)	Ref.
1	MCS-HOF	**$H_2C_2O_4·2H_2O$, $C_{10}H_8N_2$**	**NG*, 50 Hz-10 s**	**94.82**	**This work**
2	Ni-MOF	$Ni(CH_3COO)_2·4H_2O$, H_3BTC	NG, 50 Hz-1 min	65.57	3
3	PFC-1	H_4TBAPy, EtOH	LAG*, 20 Hz-20 min	92.4	4
4	MIL-88B	$Fe(NO_3)_3·9H_2O$, H_2BDC， EtOH	LAG, 500 rpm-1 h	45.1	5
5	MOF-14	$Cu_3(BTB)_2$, BTB=4,4',4"-benzenetribenzoate, EtOH	LAG, 25 Hz-10 min/ 40 Hz-15 min	57.01	6
6	SPCP-Zn	$Zn(OAc)_2$, K_2CO_3	NG, high-speed vibrating ball miller (300 W motor power)，20 min	91	7
7	MIL-78	$C_6H_3(COOH)_3$, Yttrium hydride	NG, 1725 and 1060 rpm-5 min~420 min	-	8
8	ZIF-8	ZnO, Hmim	NG, 100 rpm-96 h	80	9
9	ZIF-8	ZnO, Him, HmeIm, HetIm, LAG、EtOH、DMF、DEF, NH_4NO_3、$NH_4CH_3SO_3$、 KNO_3、$(NH_4)_2SO_4$、K_2SO_4	LAG, ILAG*, 30 Hz-5~60 min	-	10
10	MOF-5	$Zn(OAc)_2·2H_2O$, H_2BDC	NG, 900-1100 r min^{-1}, 30~90 min	-	11
11	UIO-66	ZrO_2, $C_8H_6O_4$, DMF/MeOH	30 Hz-90/180 min	-	12
12	MIL-100(Fe)	$Fe(NO_3)_3·9H_2O$, $C_9H_6O_6$	NG, milling in mortar for 10 min, Crystallisation at 160 °C for 4 h	93	13
13	HKUST-1	$Cu(OAc)_2·H_2O$, H_3BTC	NG, 25 Hz-5~25 min	-	14
14	Ln-MIL-78	$C_6H_3(COOH)_3$, $[Ln_2(CO_3)_3·xH_2O]$（Ln=Eu、Gd、Tb and Dy）	NG-2 h	-	15
15	Fe-MOF-Pd	NH_2-BDC, $Fe(NO_3)_3·9H_2O$, ZrO_2, TMAOH	LAG-1 h	-	16

16	UiO-67-bpy-Cu	$Zr_6O_4(OH)_4(C_6H_5CO_2)_{12}$, $CuBr_2$,	LAG, 30 Hz-3 h	-	[17]
17	OPA-MOF	$FeCl_3·6H_2O$, $K_2HPO_4·3H_2O$, $(NH_4)_2HPO_4$, $H_2C_2O_4·2H_2O$, CH_4N_2O	NG, 600 r/min-12 min, 333 k-10 h	-	[18]
18	$Zn_2(5\text{-aip})_2$ (bpy)	$Zn(CH_3COO)_2·2H_2O$, 5-aip, 4,4′-bipyridine	NG, 40 Hz-1~5 min	60	[19]

* **NG** for solvent-free grinding, **LAG** for liquid-assisted grinding，**ILAG** for ionic liquid assisted grinding.

Table S4. MCS-HOF yields obtained from scale-up experiments at a frequency of 50 Hz for a time of 10 s.

Sample	Yield(%)
MCS-HOF-50Hz-10s-Scale up	90.23

Supplementary Reference.

1. B. Lü, Y. Chen, P. Li, B. Wang, K. Müllen and M. Yin, *Nat. Commun.*, 2019, **10**, 767.
2. S. Wang, S. Li, J. Xiong, Z. Lin, W. Wei and Y. Xu, *Chem. Commun.*, 2020, **56**, 7399–7402.
3. R. Zhang, C.-A. Tao, R. Chen, L. Wu, X. Zou and J. Wang, *Nanomaterials*, 2018, **8**, 1067.
4. Q. Yin, E. V. Alexandrov, D. Si, Q. Huang, Z. Fang, Y. Zhang, A. Zhang, W. Qin, Y. Li, T. Liu and D. M. Proserpio, *Angew. Chem. Int. Ed.*, 2022, **61**, e202115854.
5. S. Hou, Y. Wu, L. Feng, W. Chen, Y. Wang, C. Morlay and F. Li, *Dalton Trans.*, 2018, **47**, 2222–2231.
6. M. Klimakow, P. Klobes, A. F. Thünemann, K. Rademann and F. Emmerling, *Chem. Mater.*, 2010, **22**, 5216–5221.
7. P. Zhang, H. Li, G. M. Veith and S. Dai, *Adv. Mater.*, 2015, **27**, 234–239.
8. N. K. Singh, M. Hardi and V. P. Balema, *Chem. Commun.*, 2013, **49**, 972–974.
9. S. Tanaka, K. Kida, T. Nagaoka, T. Ota and Y. Miyake, *Chem. Commun.*, 2013, **49**, 7884.
10. P. J. Beldon, L. Fábián, R. S. Stein, A. Thirumurugan, A. K. Cheetham and T. Friščić, *Angew. Chem. Int. Ed.*, 2010, **49**, 9640–9643.
11. D. Lv, Y. Chen, Y. Li, R. Shi, H. Wu, X. Sun, J. Xiao, H. Xi, Q. Xia and Z. Li, *J. Chem. Eng. Data*, 2017, **62**, 2030–2036.
12. K. Užarević, T. C. Wang, S.-Y. Moon, A. M. Fidelli, J. T. Hupp, O. K. Farha and T. Friščić, *Chem. Commun.*, 2016, **52**, 2133–2136.
13. L. Han, H. Qi, D. Zhang, G. Ye, W. Zhou, C. Hou, W. Xu and Y. Sun, *New J. Chem.*, 2017, **41**, 13504–13509.
14. W. Yuan, A. L. Garay, A. Pichon, R. Clowes, C. D. Wood, A. I. Cooper and S. L. James, *CrystEngComm*, 2010, **12**, 4063.
15. T. Alammar, I. Z. Hlova, S. Gupta, V. Balema, V. K. Pecharsky and A.-V. Mudring, *Dalton Trans.*, 2018, **47**, 7594–7601.
16. D. He, H. Niu, S. He, L. Mao, Y. Cai and Y. Liang, *Water Res.*, 2019, **162**, 151–160.
17. H. Ali-Moussa, R. Navarro Amador, J. Martinez, F. Lamaty, M. Carboni and X. Bantreil, *Mater. Lett.*, 2017, **197**, 171–174.
18. Y. Du, X. Xu, F. Ma and C. Du, *Polymers*, 2021, **13**, 561.
19. Y. Chen, H. Wu, Y. Yuan, D. Lv, Z. Qiao, D. An, X. Wu, H. Liang, Z. Li and Q. Xia, *Chem. Eng. J.*, 2020, **385**, 123836.